A hybrid FV/FD scheme for a novel conservative form of extended Boussinesq equations for waves in porous media

Van Nghi Vu, Maria Kazolea, Van Khoi Pham, Changhoon Lee

HAL Id: hal-03778750
https://hal.inria.fr/hal-03778750

Submitted on 16 Sep 2022

A hybrid FV/FD scheme for a novel conservative form of extended Boussinesq equations for waves in porous media

Van Nghi Vu, Maria Kazolea, Van Khoi Pham, Changhoon Lee

aInstitute of Civil Engineering, Ho Chi Minh City University of Transport, 2 Vo Oanh, Binh Thanh Dist., Ho Chi Minh City, 700000, Vietnam
bINRIA, Univ. Bordeaux, 200 Avenue de la Vieille Tour, Talence cedex, 33405, France
cDepartment of Civil Engineering, Vietnam Maritime University, 484 Lach Tray, Le Chan Dist., Hai Phong City, 15000, Vietnam
dDepartment of Civil and Environmental Engineering, Sejong University, 209 Neungdong-ro, Gwangjin-gu, Seoul, 05006, South Korea

Abstract

This paper introduces a conservative form of the extended Boussinesq equations for waves in porous media. This model can be used in both porous and non-porous media since it does not requires any boundary condition at the interface between the porous and non-porous media. A hybrid Finite Volume/Finite Difference (FV/FD) scheme technique is used to solve the conservative form of the extended Boussinesq equations for waves in porous media. For the hyperbolic part of the governing equations, the FV formulation is applied with Riemann solver of Roe approximation. Whereas, the dispersive and porosity terms are discretized by using FD. The model is validated with experimental data for solitary waves interacting with porous structures and a porous dam break of a one-dimensional flow.

Keywords: conservative form, extended Boussinesq equations, FV/FD scheme, porous media, porous dam break

1. Introduction

In coastal and ocean engineering computations, the Boussinesq-type (BT) equations have become the most favorable approximations of the Navier-Stokes equations. In contrast to the also widely used nonlinear shallow water equations (NSWE), the BT mathematical models have larger capabilities on the approximation of short waves generation and propagation, due to the existence of the dispersive terms in those models. Peregrine [1] was the first author who derived the weakly dispersive Boussinesq equations for long waves. In efforts to extend the Boussinesq equations to be valid in deeper areas, two approaches were presented by Madsen and Sørensen (MS) [2] and Nwogu [3]. Madsen and Sørensen [2] employed more dispersive terms in the momentum equations while Nwogu [3] used the particle velocity at a specific depth. Both sets of equations are weakly nonlinear weakly dispersive and are derived under the assumption of clean water. More recently, several authors developed fully nonlinear Boussinesq models [4][5][6], which can account for the nearshore wave circulation. However, these fully nonlinear Boussinesq models took into account higher powers of nonlinear parameters which is computationally expensive compared to the weakly nonlinear extended Boussinesq model.

The past decades have noticed some notable efforts on modeling the hydrodynamics interactions of waves and porous structures using BT models. The porous structures, e.g., the porous breakwaters,

are used to dissipate the wave energy at the coastlines, see for example [7, 8, 9, 10, 11, 12, 13, 14, 15, 16, 17]. Abbott et al. [7] were the pioneer researchers who derived the Boussinesq equations in porous breakwaters with the energy dissipation in the drag resistance term but without yet considering the inertial resistance term. When the drag resistance term is neglected, the Abbott's Boussinesq equations are reduced to Peregrine's Boussinesq equations for clean water waves. Various works in the literature attempted to include the inertial and drag resistance simultaneously, see for example [8, 11, 12, 15] with satisfactory results in the dissipating efficiency of various porous media in real coastal problems. The limitation of these works is that the BT equations used were developed in a non-conservative form, using non-conservative numerical schemes. This results in the inability of the schemes to properly handle shock waves and other discontinuity problems like wave breaking at coastal structures or surf zones.

In terms of numerical methods for weakly dispersive BT equations, there are lots of efforts related to the finite difference (FD), finite element (FE) and finite volume (FV) methods. For an extensive review on the topic we refer the interested readers to [18] and [19, 20]. The FV method requires less computational effort compared to the FE method and the nonlinear advection terms can be handled easier compared to the FD method. Recently the combination of FV and FD methods have been introduced for BT equations in order to exploit the flexibility and shock capturing capabilities of the FV method and the easiness of the FD in the discretization of the higher order terms. Some notable hybrid approaches for BT models, in clean water, can be found in [21, 22, 23, 6, 24, 25, 26, 27, 19] and references therein.

The objective of this work is to develop a relevant hybrid FV/FD numerical scheme for the extended Boussinesq equations for waves in porous media of Vu et al. [15]. These Boussinesq equations, which follow the weakly nonlinear weakly dispersive Madsen and Sørensen's Boussinesq equations [2], include drag resistance as well as inertial resistance to compute correctly the short wave dissipation in porous media. Also, the BT equations are derived following the conservative form, which can deal with the nearshore waves [23] like breaking waves.

The manuscript is organized as follows. The extended Boussinesq equations for porous media in the conservative form are developed in section 2. In section 3, the extended Boussinesq equations are discretized using the hybrid FV/FD scheme where the FV scheme solves the advective terms and the FD scheme solves the dispersive and porosity terms. Section 4 briefly describes the wave breaking technique along with the boundary conditions used in this work. Finally in section 5, we investigate our model using standard benchmark test cases for waves in porous media. The manuscript is concluded by a discussion and an outlook on future work.

2. Governing equations

In this work as a starting point we use the extended BT model of [15]. Their model has some advantages in simulations of waves inside and outside porous media. The model does not need to specify any matching condition at the boundary of the porous medium interface. The model has shown its accuracy to the experimental data and numerical results of [14]. However the model is unable to simulate wave breaking and waves in surf zones. This also has a consequence in the simulation of the run-up of the waves on the coasts. In order to overcome this issue we re-write the model of [15] in an one-dimensional conservative formulation. More precisely we have

$$\eta_t + q_x \;=\; 0 \tag{1}$$

$$\beta\left[q_t + \left(\frac{q^2}{H}\right)_x\right] + \alpha q + gH\eta_x \;=\; \beta d^2\left(B + \frac{1}{3}\right)q_{xxt} + Bgd^3\eta_{xxx} + dd_x\left(\frac{1}{3}\beta q_{xt} + 2Bgd\eta_{xx}\right)$$

$$+\;\; \alpha\left(B + \frac{1}{3}\right)d^2 q_{xx} + \frac{1}{3}\alpha dd_x q_x \tag{2}$$

where $H = d + \eta$ is the total water depth, d is the still water level and η the water surface elevation. We write the momentum as $q = Hu$ with u being the horizontal seepage velocity and g the gravitational acceleration. B (=1/18) is the tuning parameter to extend capabilities of the model to the deeper areas. See also figure 1 for the parameters' description.
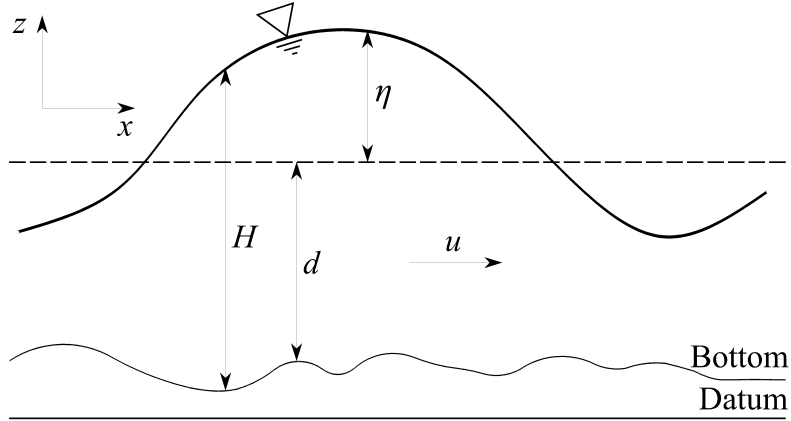

Figure 1: Sketch of the free surface flow problem and main parameter description

α and β are the drag and inertial coefficients respectively given by

$$\alpha \;=\; \alpha_l\left(\frac{1-\lambda}{\lambda}\right)^2 \frac{\nu}{d_s^2} + \alpha_t \frac{1-\lambda}{\lambda}\frac{1}{d_s}|u| \tag{3}$$

$$\beta \;=\; 1 + (1-\lambda)\kappa \tag{4}$$

where λ is the porosity, κ is the added mass coefficient, α_l and α_t are the coefficients which represent the laminar and the turbulent flow respectively. ν is the kinematic viscosity of the water and d_s is the size of the porous material. We have to highlight that if no porosity gradients exists in the domain then the system of equations (1) and (2) degenerates to the classical system of weakly non linear weakly dispersive equations of Madsen and Sørensen [2].

In a more compact form, and following the work in [19], the system can be written as:

$$\mathbf{U}_t + \mathbf{F}(\mathbf{U})_x = \mathbf{S}_f + \mathbf{S}_l \tag{5}$$

3

with

$$\mathbf{U} = \begin{bmatrix} H \\ P \end{bmatrix}, \ \mathbf{F(U)} = \begin{bmatrix} q \\ \frac{q^2}{H} + \frac{1}{2\beta}gH^2 \end{bmatrix}, \ \mathbf{S_f} = \begin{bmatrix} 0 \\ N_m^2 \frac{u|u|}{\beta H^{4/3}} \end{bmatrix} \tag{6}$$

$\mathbf{U}$ is the vector of the unknown variables, $\mathbf{F(U)}$ the non linear flux vector and $\mathbf{S}_f$ the friction term with N_m being the Manning coefficient. The last term in the right hand side of (5) contains both dispersive and porosity terms and equals to

$$\mathbf{S}_l = \frac{1}{\beta} \begin{bmatrix} 0 \\ \psi - \alpha q \end{bmatrix} \tag{7}$$

where $\psi = \psi_d + \psi_p$ in which

$$\psi_d = Bgd^3\eta_{xxx} + 2d^2 d_x Bg\eta_{xx} \ \text{ and } \ \psi_p = \frac{1}{3}\alpha d d_x q_x + \left(B + \frac{1}{3} \right)\alpha d^2 q_{xx}. \tag{8}$$

P is the velocity like function and has all the time derivatives in the momentum equation and is defined as

$$P = q - \left((B + \frac{1}{3})d^2 q_{xx} - \frac{1}{3}dd_x q_x \right). \tag{9}$$

3. Numerical scheme

We use a hybrid FV/FD numerical scheme to solve the system (5). This scheme is based on the one used in [19] but of course further work is required since the authors in [19] are solving the MS equations on clean water, without porosity. We will use the FV formulation for the hyperbolic part of the equations and the FD for the remaining terms. Before applying the discretization in (5) we will examine briefly some of the properties of the homogeneous system, meaning that the source terms are zero. The Jacobian matrix of (5) is

$$\mathbf{J} = \frac{\partial \mathbf{F(U)}}{\partial \mathbf{U}} = \begin{bmatrix} 0 & 1 \\ -u^2 + \frac{g}{\beta}H & 2u \end{bmatrix} \tag{10}$$

The two eigenvalues of the matrix are real and read as

$$\lambda_1 = u + c, \ \lambda_2 = u - c \tag{11}$$

where the celerity $c = \sqrt{(g/\beta)H}$. The corresponding eigenvectors are:

$$\mathbf{r_1} = \begin{bmatrix} 1 \\ u + c \end{bmatrix}, \ \mathbf{r_2} = \begin{bmatrix} 1 \\ u - c \end{bmatrix} \tag{12}$$

The system is hyperbolic but has slightly different eigenvalues and eigenvectors than the classical shallow water equations. Of course when there is no porosity, i.e., $\beta = 1$, the eigenvalues and eigenvectors are those of the shallow water equations. This property makes it ideal for using an approximate Riemann solver in the FV discretization in order to compute the numerical fluxes that occur.

4

3.1. Numerical treatment for the hyperbolic part

Following the procedure required for a FV scheme and after integrating (5) over a control volume $C_i = [x_{i-1/2}, \ x_{i+1/2}] \times [t^n, \ t^{n+1}]$ of dimensions $\Delta x = x_{i+1/2} - x_{i-1/2}$ and $\Delta t = t^{n+1} - t^n$, we obtain the semi-discrete form for the hyperbolic part of the equations:

$$\frac{\Delta \mathbf{U}_i^n}{\Delta t} = -\frac{1}{\Delta x} \left[\mathbf{F}_{i+1/2}^n - \mathbf{F}_{i-1/2}^n \right].$$
(13)

$\mathbf{U_i^n}$ is the approximate cell average of $\mathbf{U}$ in the control volume at time t^n, i.e. $\mathbf{U}_i^n = \frac{1}{\Delta x} \int_{C_i} \mathbf{U}(x, t^n) dx$. $\mathbf{F}_{i\pm1/2}^n$ are the numerical fluxes in each interface of the control volume C_i. The numerical fluxes are computed using the approximate Riemann solver of Roe [28]. To define a linearized Riemann solver we have to consider the linearized form of the homogeneous system (5) and replace the Jacobian matrix by some matrix $\hat{\mathbf{J}}$ depending on the left ($\mathbf{U_l}$) and right ($\mathbf{U_r}$) states. This matrix should satisfy three properties: consistency, hyperbolicity and conservation. The last one defines the approximate Riemann solver of Roe while the first two are essential for all the approximate solvers. A general derivation, for hyperbolic systems, can be found in [28, 29]. Here we follow a simple way by applying the conservation property that states

$$\hat{\mathbf{J}}(\mathbf{U_r}, \mathbf{U_l})(\mathbf{U_r} - \mathbf{U_l}) = \mathbf{F}(\mathbf{U_r}) - \mathbf{F}(\mathbf{U_l}).$$
(14)

We look for a matrix $\hat{\mathbf{J}}$ evaluated in an average state: $\hat{\mathbf{J}}(\mathbf{U_r}, \mathbf{U_l}) = \hat{\mathbf{J}}(\hat{\mathbf{U}})$. This ensures consistency and hyperbolicity if $\hat{\mathbf{U}}$ is an average of the left and right states. The eigenvalues and the eigenvectors of the linearized system, evaluated at an average state are:

$$\hat{\lambda}_1 = \hat{u} + \hat{c}, \ \hat{\lambda}_2 = \hat{u} - \hat{c}$$
(15)

and

$$\hat{\mathbf{r}_1} = \begin{bmatrix} 1 \\ \hat{u} + \hat{c} \end{bmatrix}, \ \hat{\mathbf{r}_2} = \begin{bmatrix} 1 \\ \hat{u} - \hat{c} \end{bmatrix}$$
(16)

respectively. $\hat{c}$ is the average celerity and equals $\sqrt{(g/\beta)H}$. The next step is to decompose the jump $(\mathbf{U_r} - \mathbf{U_l}) = \alpha_1 \hat{\mathbf{r}_1} + \alpha_2 \hat{\mathbf{r}_2} = \hat{\mathbf{R}}\alpha$. $\hat{\mathbf{R}}$ is the eigenvector matrix evaluated at the average state and $\alpha = [\alpha_1 \ \alpha_2]$ can be found by solving the linear system $\alpha = \hat{\mathbf{R}}^{-1}(\mathbf{U_r} - \mathbf{U_l})$. This gives us the expressions:

$$\alpha_1 = \frac{-(\hat{u} - \hat{c})(H_r - H_l) + (q_r - q_l)}{2\hat{c}}, \ \ \alpha_2 = \frac{(\hat{u} + \hat{c})(H_r - H_l) + (q_r - q_l)}{2\hat{c}}.$$
(17)

Finally, in order to derive the average values of Roe, $\hat{H}$ and $\hat{u}$ we exploit (14) written in the form $\hat{\mathbf{J}}(\hat{\mathbf{U}})(\mathbf{U_r} - \mathbf{U_l}) = \mathbf{F}(\mathbf{U_r}) - \mathbf{F}(\mathbf{U_l})$. The second equation of this system writes as:

$$(-\hat{u}^2 + \frac{g\hat{H}}{\beta})(H_r - H_l) + 2\hat{u}(q_r - q_l) = H_r u_r^2 - H_l u_l^2 + \frac{g}{2}(H_r^2 - H_l^2).$$
(18)

We separate the terms involving g and we get

$$\hat{H} = \beta \frac{H_r + H_l}{2}$$
(19)

while for those that they do not involve g we write:

$$\hat{u} = \frac{\sqrt{H_r}u_r + \sqrt{H_l}u_l}{\sqrt{H_r} + \sqrt{H_l}}. \tag{20}$$

We can see that the Roe average state for the velocity is the same as one of the classical nonlinear shallow water equations while the Roe averaged state for the water height is the same as one of the shallow water multiplied by β. So, the numerical fluxes are written in a classic way as:

$$\mathbf{F}_{i+1/2} = \frac{1}{2}\left(\mathbf{F}^r_{i+1/2} + \mathbf{F}^l_{i+1/2}\right) - \frac{1}{2}|\hat{\mathbf{J}}|_{1+1/2}\left(\mathbf{U}^r_{1+1/2} - \mathbf{U}^l_{1+1/2}\right) \tag{21}$$

where $|\hat{\mathbf{J}}|_{i+1/2} = [\hat{\mathbf{X}}|\hat{\mathbf{\Lambda}}|\hat{\mathbf{X}}^{-1}]_{i+1/2}$ and $\hat{\mathbf{X}}_{i+1/2}$ is the right eigenvector matrix and $\hat{\mathbf{\Lambda}}_{i+1/2}$ the diagonal matrix with the eigenvalues in the diagonal.

Higher order discretization: Up to now if we set $\mathbf{U}_l = \mathbf{U}_i$ and $\mathbf{U}_r = \mathbf{U}_{i+1}$ then we resolve to a first order scheme in time. Higher order accuracy in the computation of the numerical fluxes is achieved by constructing the left and right cell interface values using a third order MUSCL-type extrapolation scheme [30, 31]. The reconstruction is implemented on the primitive variables. More details on the procedure can be found in [32].

3.2. Discretization of the dispersive and porosity terms

The terms of the right hand side $\mathbf{S}_l$ that contains some dispersive and porosity terms are discretized by using the Finite Difference (FD) technique. We have to be careful in the discretization of the equations as we do not want the leading truncation error terms derivatives to be of the same order as of those contained in the equations. These terms will affect the dispersion relation significantly the reader can refer to [33, 34] and [32] for more details. In this work we discretize the dispersive and porosity terms using fourth order central FD approximations for the first order derivatives, third order central FD approximations for the third order derivatives and second order central FD approximations for the second order derivatives. We write the cell average of second term, S_l, of (7) :

$$(S_l)_i = \frac{1}{\Delta x}\int_{C_i}\frac{1}{\beta}(\psi - \alpha q)dx. \tag{22}$$

The second part of the equation is by default $\alpha_i q_i$. To compute the first part of the above term we substitute the cell average values into the Taylor series and we express a cell average value with values defined at the cell interfaces [35, 36]. After some calculus we discretize the term ψ using

$$\begin{aligned}
(f_i)_x &= \frac{f_{i-2} - 8f_{i-1} + 8f_{i+1} - f_{i+2}}{12\Delta x} + O(\Delta x^2), \\
(f_i)_{xx} &= \frac{f_{i-1} - 2f_i + f_{i+1}}{\Delta x^2} + O(\Delta x^2), \\
(f_i)_{xxx} &= \frac{-f_{i-2} + 2f_{i-1} - 2f_{i+1} + f_{i+2}}{2\Delta x^3} + O(\Delta x^3).
\end{aligned} \tag{23}$$

where, f_i, f_{i+1}, ..., are the average values, so we get

$$(\psi_d)_i = -\frac{Bgd_i^3}{2\Delta x^3}\left(\eta_{i+2} - 2\eta_{i+1} + 2\eta_{i-1} - \eta_{i-2}\right) - \frac{Bgd_i^2}{6\Delta x^3}\left(d_{i-2} - 8d_{i-1} + 8d_{i+1} - d_{i+2}\right)\left(\eta_{i-1} - 2\eta_i + \eta_{i+1}\right) \tag{24}$$

For the porosity terms ψ_p we again use (23) to approximate the derivatives.

6

3.3. Time integration and Recovery of the velocity field

The temporal domain is discretized by a set of non-overlapping cells $[t^n, \ t^{n+1}]$. We denote $\Delta t^{n+1} = t^{n+1} - t^n$ which is computed by means of the CFL condition

$$\Delta t^{n+1} = CFL \frac{\Delta x}{max_i(|u_i^n| + \sqrt{(g/\beta)h_i^n})}. \tag{25}$$

The integration scheme that we use is the fourth order Adams-Bashforth/Adams-Moulton predictor-corrector method which requires two stages. The scheme is widely used for Boussineq modeling and full details can be found in [19] and the references therein. In both steps we obtain the values for H_i and P_i from which we have to extract the values of the momentum q_i and consequently the velocity u_i. In order to discretize (9) we use the approximations form (23) for the existing first and second order derivatives in P. We also use the central FD approximation for $(q_i)_x$. Equation (9) results in a tridiagonal system which is exactly the same as the one obtained from the MS equations in clean water [19]. This is expected since no porosity terms are involved in the velocity like function. For the sake of completeness we repeat here the form of the tridiagonal linear system of equations:

$$\gamma_i q_{i-1} + \delta_i + \epsilon_i q_{i+1} = P_i \tag{26}$$

with

$$\gamma_i = -k_1 + \frac{k_2}{72}, \ \delta_i = 1 + 2k_1, \ \epsilon_i = -k_1 - \frac{k_2}{72} \tag{27}$$

in which

$$k_1 = \left(B + \frac{1}{3}\right)\left(\frac{d_i^2}{\Delta x^2}\right) \text{ and} \tag{28}$$

$$k_2 = \frac{d_i^2}{\Delta x^2}(d_{i-2} - 8d_{i-1} + 8d_i - d_{i+2}). \tag{29}$$

We use the Lapack-Linear Algebra Package to efficiently solve the tridiagonal system in each sub time step.

4. Boundary conditions and wave breaking treatment

The boundary conditions used in all the test cases are solid wall boundary conditions. For this reason three boundary nodes in the first and last cell are introduced and their values are determined through the boundary conditions. More precisely we use an odd and even extrapolation for H while the velocity in the ghost cells is defined as the opposite value of the velocity from the interior. The boundary conditions are introduced in the linear system before solving in order to obtain the velocity field.

Last but not least we briefly describe the wave breaking treatment that we use. Following [20, 32, 22], among others, a hybrid strategy is implemented in the scheme to handle wave breaking. The hybrid wave breaking strategy is widely used with BT models due to its easy implementation. The interested reader can find more information on the topic in [37, 38]. The treatment can be divided into two parts. First the detection and characterization of breaking regions through explicit criteria and second the application of the NSWE in the breaking regions and the MS equations elsewhere. We remind the reader that we obtain the NSWE for our model by simply omitting the dispersive terms. Following [20] we use the combination of the two local criteria for the following mechanism:

7

1. $|\eta_t| \geq \gamma\sqrt{gH}, \ \gamma \in [0.35, \ 0.65]$, the surface variation criterion
2. $||\nabla\eta|| \geq \tan(\phi_c), \ \phi_c = 30°$ is the critical angle value, the local slope angle criterion.

The values of γ and ϕ_c depend on the type of breaker. The first criterion flags for breaking when η_t is positive, since breaking starts on the front face of the wave, while the second criterion, acting complementary to the first, is useful for the detection of hydraulic jumps. Moreover, the estimation of the Froude number of the wave is used to established when to switch of the breaking and to detect non-breaking bores.

5. Numerical tests

In order to verify the developed model, in this study we compare our numerical results with the numerical and physical experimental data of [10]. The numerical results show good agreement with the compared data. Secondly, we compare with a porous dam-break cases of [39].

5.1. Solitary waves interaction with porous structures

In this part, the effect of the nonlinearity on the wave transmission behind a porous breakwater is verified with the experimental data of [10]. Solitary waves with amplitude of 1-3.5 cm were generated in constant water depth of 10 cm which results in the nonlinearity $\epsilon = a/d = 0.1 - 0.35$, and the surface elevations were measured 1 m in front of and 1 m behind the porous breakwater. Breakwater widths are tested for 2 cases, 15 cm and 30 cm together with two types of gravel diameter $d_s = 1.6cm$ and $d_s = 2cm$. The porosity $\lambda = 0.5$ is used in all cases. The laminar and turbulent drag coefficients are $\alpha_l = 3000$ and $\alpha_t = 3$, respectively.

5.1.1. Effect of the nonlinearity

Figure 2 shows the transmission and reflection coefficients (T and R, respectively) of the experimental data and numerical results when the nonlinearities increase from 0.1 to 0.35. In general, the transmission coefficients have the same decreasing trend when the nonlinearities increase due to high nonlinearity effect. Meanwhile, the reflection coefficients increase with small values of nonlinearity (i.e., $a/d < 0.15$). However, when the nonlinearity increases, the reflection coefficients decrease due to the frequency dispersion induced by the porous breakwater and the nonlinearity effect becomes more noticeable. The reflected solitary waves include a prominent wave and some trailing waves. When the nonlinearity increases, the trailing wave heights increase which may reduce the reflection wave height in front of the porous breakwater. This phenomenon has been explained in [40].

In comparison to the non-conservative form of Boussinesq model for waves in porous media of [15], the conservative form model in this study shows its advantage in the reflection coefficients.

5.1.2. Effect of the width of the porous breakwater

The reflection and transmission of solitary waves to a porous breakwater are determined in some more cases when we change the breakwater width. The porous breakwater conditions are the same as the previous cases, such as $\lambda = 0.5$, $\alpha_l = 3000$ and $\alpha_t = 3$. Lynett et al. (2000) [10] did the physical experiment for two breakwater widths ($b/d = 1.5$ and $b/d = 3$). We want to investigate how far the reflection and transmission of the incident solitary wave are affected by the porous breakwater width. The numerical simulations are executed for more cases with various breakwater widths. The breakwater
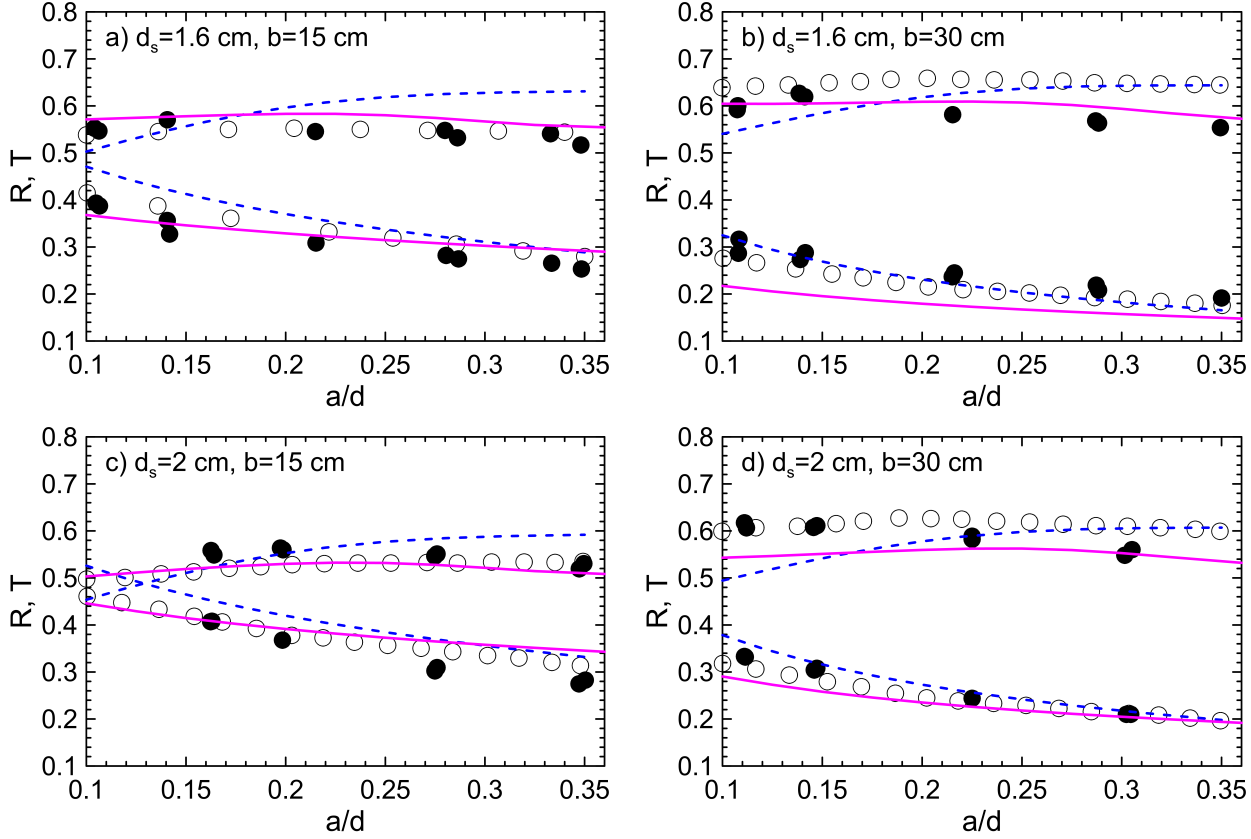
Figure 2: Reflection and transmission of solitary waves to a porous breakwater. Line definition: filled circle = Lynett et al.'s experiment; blank circle = Lynett et al.'s model; dashed line = [15] (non conservative form); solid line = conservative form

width is from 1 to 3.5 times the water depth ($b/d = 1 - 3.5$). It can be seen in figure 3 that when the breakwater width increases, the reflection slightly increases whereas the decrease of the transmission wave is more significant. The nonlinearities for both cases (figures 3a and 3b) are almost the same, the gravel diameters are different from each other and selected from the physical experiment of [10].

5.2. Porous dam-break

The advantage of the conservative form of the porous model is illustrated in this section when the model is simulated for porous dam-break cases. The experiments of [39] were carried out in a fish tank with the dimensions 44cm x 89.2cm x 58cm (width x length x height). A porous dam was placed at the middle of the fish tank with a length of 29 cm (figure 4).

There were two types of porous dam used for the experiments: the first one was filled with crushed stones of 1.59 cm diameter and a porosity of 0.49, the latter was filled with glass beads of 0.3 cm diameter and a porosity of 0.39. At initial stage, water was hold in a 25cm-high reservoir which was placed 2cm in front of the porous dam. A layer of water (2.5cm deep) always remains on the bottom of the tank. When the experiment was conducted, the water column was released and interacted with the porous dam. The numerical model has been designed to validate two dam-break cases. The grid sizes were selected as $dx = dy = 1cm$.
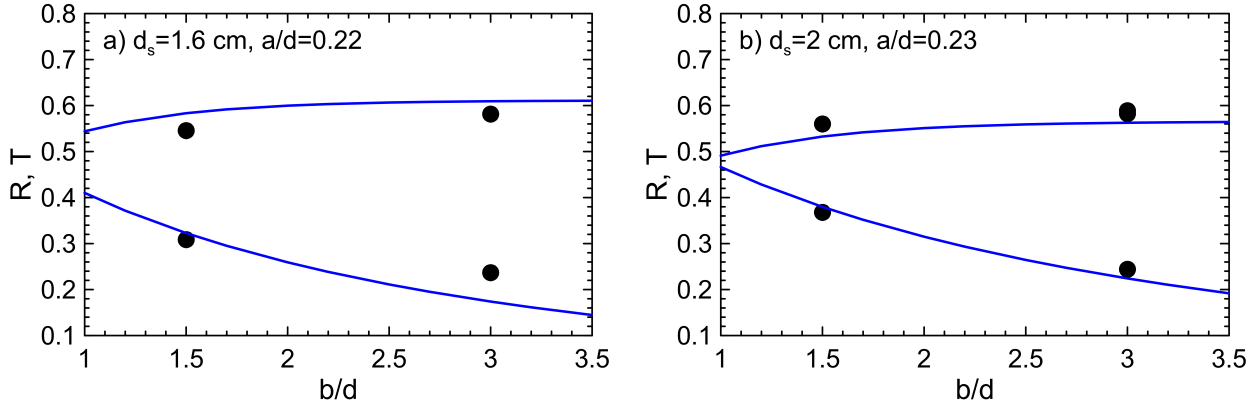
9

Figure 3: Reflection and transmission of solitary waves to a porous breakwater of Lynett et al. (2000). Line definition: filled circle = Lynett et al.'s experiment; solid line = conservative form
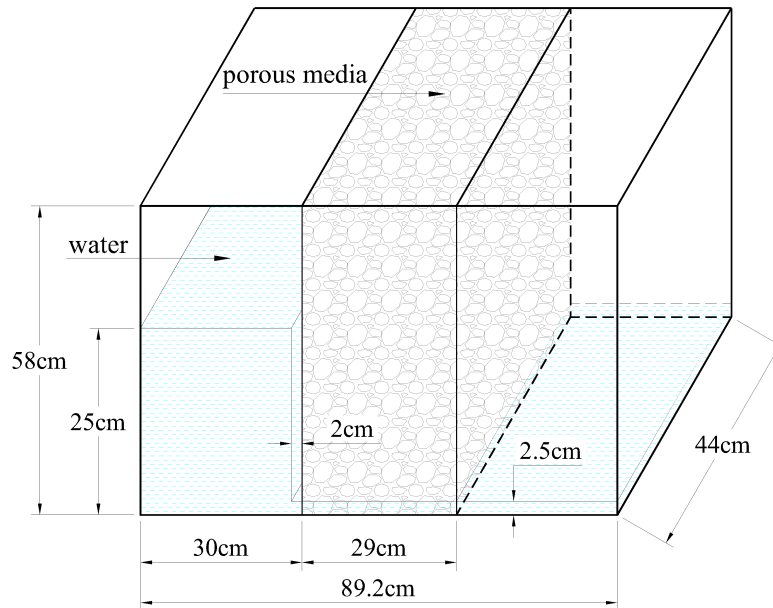

Figure 4: Geometrical configuration of the porous dam-break

5.2.1. Crushed stones dam

For the first case, the porous dam is filled with crushed stones, the porosity characteristics of the porous dam were selected to be the same as the previous test with the laminar and turbulent drag coefficients $\alpha_l = 3000$ and $\alpha_t = 3$, respectively, and the added mass coefficient $\kappa = 0.34$.

Figure 5 shows a good comparison between the numerical results and the experimental data of [39]. The wave breaking happens in front of the porous dam and the surface elevation criterion is applied as described in Section 4. This is an advantage of the conservative form of Boussinesq model for waves in porous media comparing to the non-conservative form. The non-conservative form of the Boussinesq model for waves in porous media can not simulate porous dam break cases naturally.
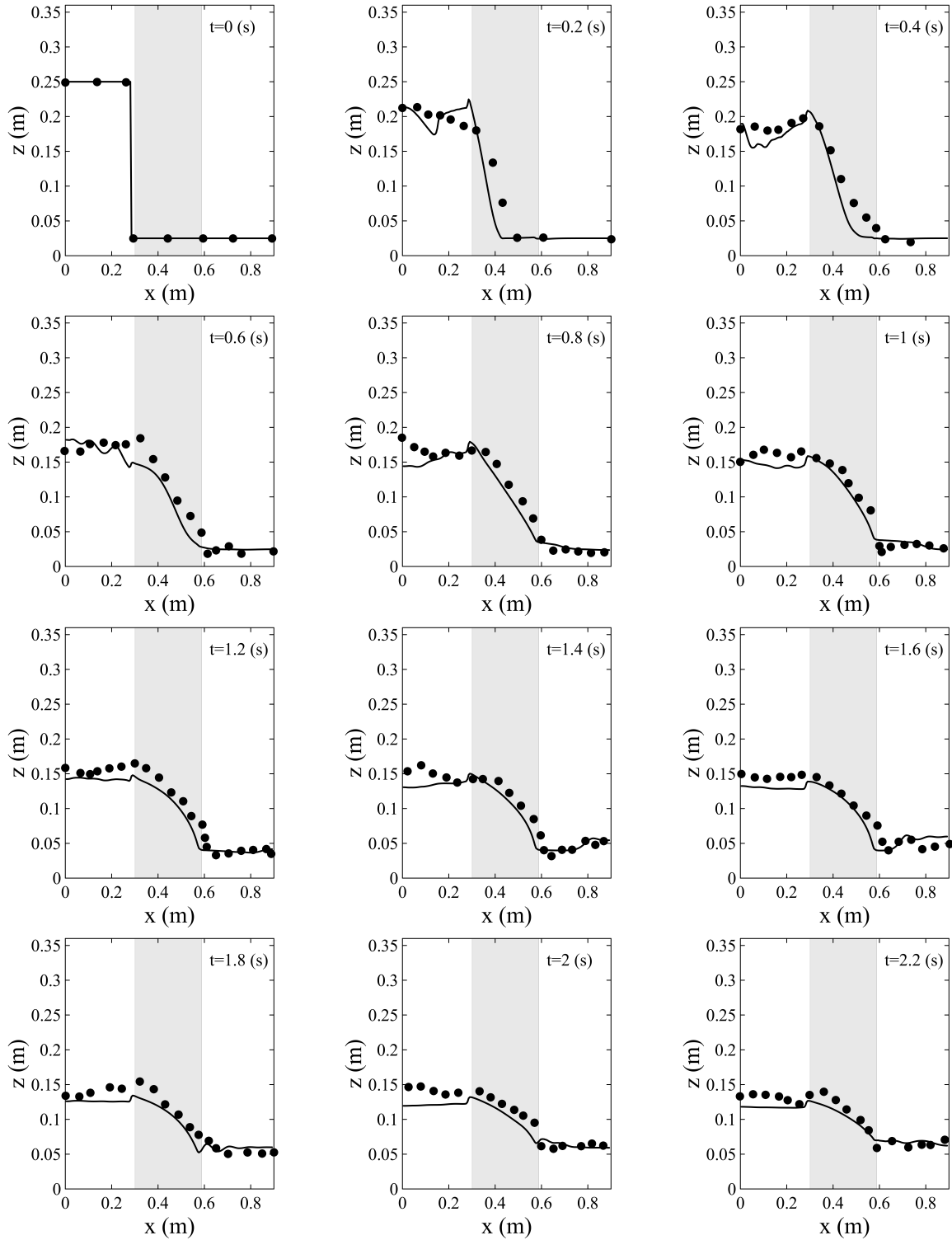
10

Figure 5: crushed stones dam-break validation. solid line: present numerical solution; solid circle: experimental data of [39]

The porosity of the dam varies from 0.19 (very dense) to 1 (non-porous) to see more details about

the variation of water flow with respect to porosities. The water surface elevations are recorded at 1 sec. When the porosity is small (i.e., $\lambda < 0.3$), the flow inside the dam is slow due to high resistance force hence the water levels behind the dam are kept unchanged. However, with larger porosities, the fluid flow is faster. Particularly, when the porosity is unity there is no dam and the water flows freely.
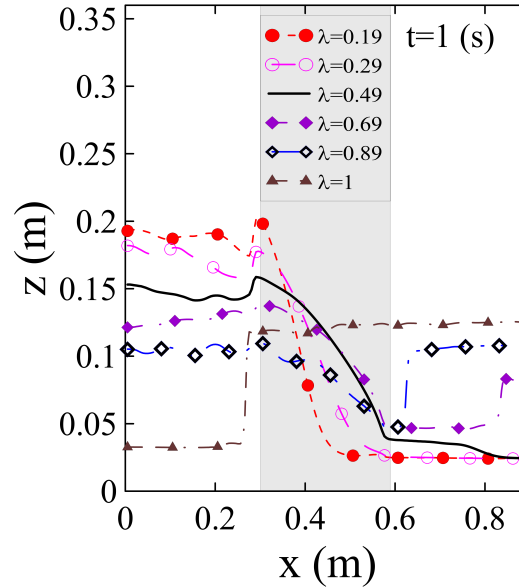

Figure 6: variation of porosities inside crushed stone dam, $\lambda = 0.19 - 1$

5.2.2. Glass beads dam

For the second experiment, the porous dam is filled with glass beads. Since the glass beads have different characteristics (shape, diameter, and porosity) from the crushed stones, the porosity characteristics of the porous dam should be modified. The drag coefficients of the porous dam were calibrated among 3 values: ($\alpha_l = 3000, \alpha_t = 3$), ($\alpha_l = 3000, \alpha_t = 0.1$), and ($\alpha_l = 600, \alpha_t = 3$). Figure 7 recorded the water surface elevation for these values at time t = 1.2 sec. It can be seen from this figure that the turbulent values do not affect the flow much, however, the laminar values are dominant. The affection of the laminar drag coefficient to the flow was also explained by [13] and [9]. Thus, we use the values of ($\alpha_l = 600, \alpha_t = 3$) for the simulation of flow through a glass bead dam.

Figure 8 illustrates the water released process from the tank through a glass bead dam. At most time steps, the numerical results show good agreement with the physical data. However, it can be seen at the last time step there is a large discrepancy in front of the glass bead dam.
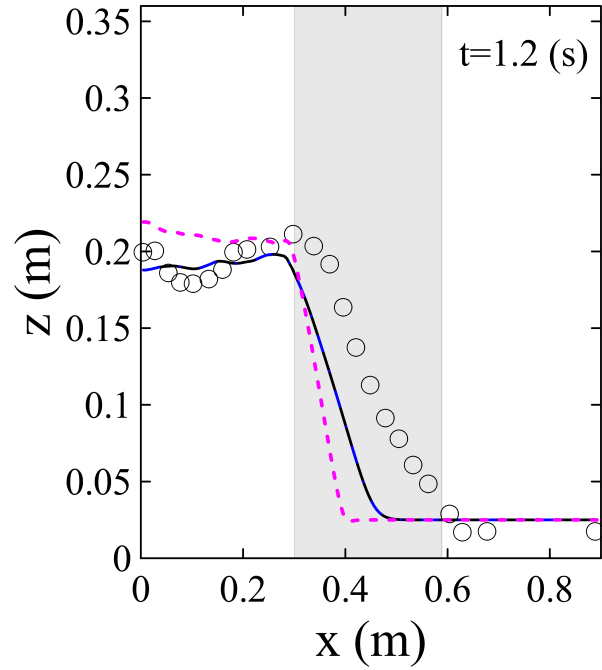
12

Figure 7: water surface elevation in glass bead case: dashed line: ($\alpha_l = 3000$, $\alpha_t = 3$); solid line ($\alpha_l = 3000$, $\alpha_t = 0.1$); dash-dotted line: ($\alpha_l = 600$, $\alpha_t = 3$); blank circle: experimental data
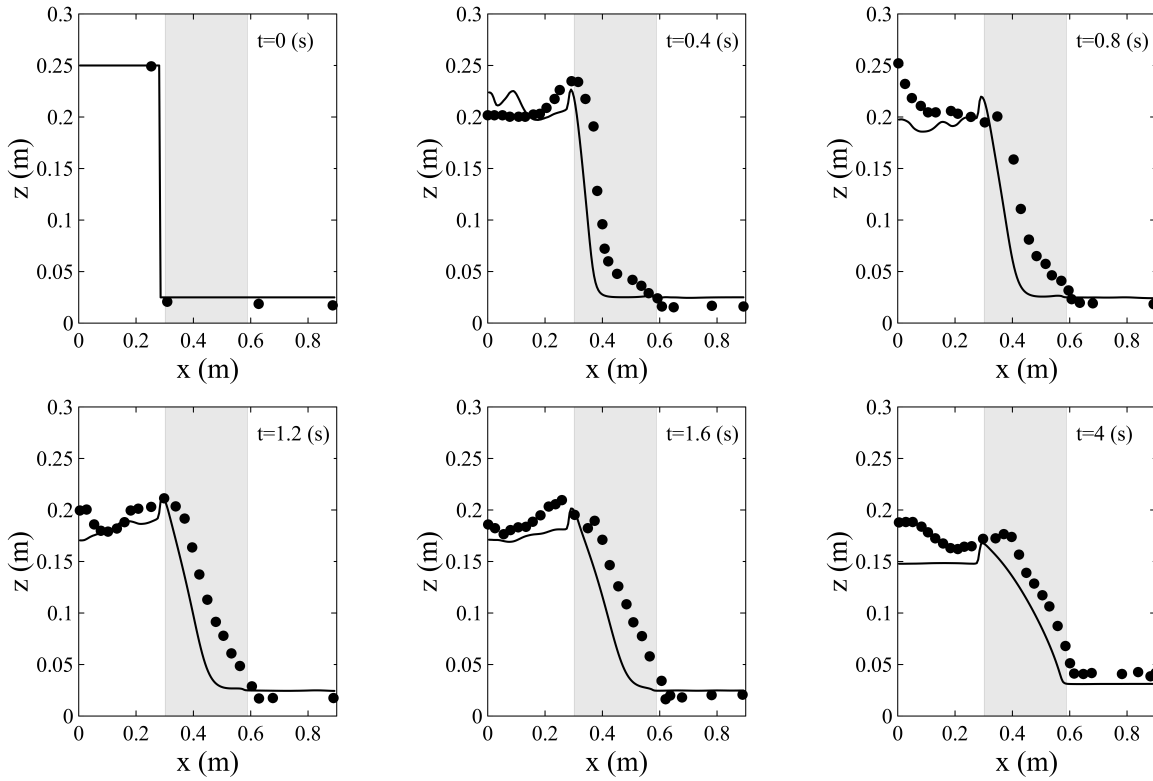

Figure 8: glass beads dam-break validation. solid line: present numerical solution; solid circle: experimental data of Lin (1998)

13

6. Concluding remarks

In this study, we introduced a conservative form of the extended Boussinesq equations for waves in porous media. In a non-conservative form for waves in porous media, the model has been developed by [15] and shows its accuracy when solitary waves interact with porous structures. In a conservative form for non-porous media, the model returns the Madsen and Sørensen equations [2] and shows its advantage on simulating wave breaking and wave run up [19]. The hybrid FV/FD numerical scheme has been applied and the numerical results were compared with the experimental data. The comparisons show that the conservative form of the extended Boussinesq equations for waves in porous media give accurate predictions in the one-dimensional case. The most important contribution of this work is that the model is able to simulate the porous dam break case, where the non-conservative form can not, see [15]. For the crushed stone dam, the turbulent drag effect is more dominant whereas for glass bead case, the laminar drag coefficient has a significant effect.

In future studies, a 2-D conservative model needs to be investigated to simulate important phenomena in coastal areas such as wave refraction and diffraction from porous structures. A multi porous layer model in conservative form should be investigated for breaking waves over porous submerged bar, waves running up on the beach and overtopping waves on porous structures.

Acknowledgment

References

[1] D. H. Peregrine, Long waves on a beach, Journal of fluid mechanics 27 (4) (1967) 815–827.

[2] P. A. Madsen, O. R. Sørensen, A new form of the boussinesq equations with improved linear dispersion characteristics. part 2. a slowly-varying bathymetry, Coastal engineering 18 (3-4) (1992) 183–204.

[3] O. Nwogu, Alternative form of boussinesq equations for nearshore wave propagation, Journal of waterway, port, coastal, and ocean engineering 119 (6) (1993) 618–638.

[4] R. E. Musumeci, I. A. Svendsen, J. Veeramony, The flow in the surf zone: a fully nonlinear boussinesq-type of approach, Coastal Engineering 52 (7) (2005) 565–598.

[5] Q. Chen, Fully nonlinear boussinesq-type equations for waves and currents over porous beds, Journal of Engineering Mechanics 132 (2) (2006) 220–230.

[6] F. Shi, J. T. Kirby, J. C. Harris, J. D. Geiman, S. T. Grilli, A high-order adaptive time-stepping tvd solver for boussinesq modeling of breaking waves and coastal inundation, Ocean Modelling 43 (2012) 36–51.

[7] M. Abbott, H. Petersen, O. Skovgaard, On the numerical modelling of short waves in shallow water, Journal of Hydraulic Research 16 (3) (1978) 173–204.

[8] E. C. Cruz, M. Isobe, A. Watanabe, Boussinesq equations for wave transformation on porous beds, Coastal Engineering 30 (1-2) (1997) 125–156.

[9] P. L.-F. Liu, P. Lin, K.-A. Chang, T. Sakakiyama, Numerical modeling of wave interaction with porous structures, Journal of waterway, port, coastal, and ocean engineering 125 (6) (1999) 322–330.

[10] P. J. Lynett, P. L.-F. Liu, I. J. Losada, C. Vidal, Solitary wave interaction with porous breakwaters, Journal of Waterway, Port, Coastal, and Ocean Engineering 126 (6) (2000) 314–322.

[11] S.-C. Hsiao, P. L.-F. Liu, Y. Chen, Nonlinear water waves propagating over a permeable bed, Proceedings of the Royal Society of London. Series A: Mathematical, Physical and Engineering Sciences 458 (2022) (2002) 1291–1322.

[12] S.-C. Hsiao, K.-C. Hu, H.-H. Hwung, Extended boussinesq equations for water-wave propagation in porous media, Journal of engineering mechanics 136 (5) (2010) 625–640.

[13] M. del Jesus, J. L. Lara, I. J. Losada, Three-dimensional interaction of waves and porous coastal structures: Part i: Numerical model formulation, Coastal Engineering 64 (2012) 57–72.

[14] J. L. Lara, M. del Jesus, I. J. Losada, Three-dimensional interaction of waves and porous coastal structures: Part ii: Experimental validation, Coastal Engineering 64 (2012) 26–46.

[15] V. N. Vu, C. Lee, T.-H. Jung, Extended boussinesq equations for waves in porous media, Coastal Engineering 139 (2018) 85–97.

[16] V. N. Vu, C. Lee, Solitary wave interaction with porous structures, Procedia Engineering 116 (2015) 834–841.

[17] V. N. Vu, T. K. Trinh, Evaluation of the wave damping by a bamboo breakwater applying a porous media model, in: Proceedings of the 2nd Vietnam Symposium on Advances in Offshore Engineering, Vol. 208, Springer Singapore, 2022, pp. 254–261.

[18] M. Brocchini, A reasoned overview on boussinesq-type models: the interplay between physics, mathematics and numerics, Proceedings of the Royal Society A: Mathematical, Physical and Engineering Sciences 469 (2160) (2013) 5–27.

[19] M. Kazolea, A. Delis, A well-balanced shock-capturing hybrid finite volume–finite difference numerical scheme for extended 1d boussinesq models, Applied Numerical Mathematics 67 (2013) 167–186.

[20] M. Kazolea, A. I. Delis, C. E. Synolakis, Numerical treatment of wave breaking on unstructured finite volume approximations for extended boussinesq-type equations, Journal of computational Physics 271 (2014) 281–305.

[21] K. Erduran, S. Ilic, V. Kutija, Hybrid finite-volume finite-difference scheme for the solution of boussinesq equations, International Journal for Numerical Methods in Fluids 49 (11) (2005) 1213–1232.

[22] M. Tonelli, M. Petti, Hybrid finite volume–finite difference scheme for 2dh improved boussinesq equations, Coastal Engineering 56 (5-6) (2009) 609–620.

[23] V. Roeber, K. F. Cheung, M. H. Kobayashi, Shock-capturing boussinesq-type model for nearshore wave processes, Coastal Engineering 57 (4) (2010) 407–423.

[24] K. Fang, Z. Zou, P. Dong, Z. Liu, Q. Gui, J. Yin, An efficient shock capturing algorithm to the extended boussinesq wave equations, Applied Ocean Research 43 (2013) 11–20.

[25] K.-z. Fang, Z. Zhang, Z.-l. Zou, Z.-b. Liu, J.-w. Sun, Modelling of 2-d extended boussinesq equations using a hybrid numerical sc-heme, Journal of Hydrodynamics, Ser. B 26 (2) (2014) 187–198.

[26] B. Tatlock, R. Briganti, R. E. Musumeci, M. Brocchini, An assessment of the roller approach for wave breaking in a hybrid finite-volume finite-difference boussinesq-type model for the surf-zone, Applied Ocean Research 73 (2018) 160–178.

[27] M. Kazolea, A. Delis, I. Nikolos, C. Synolakis, An unstructured finite volume numerical scheme for extended 2d boussinesq-type equations, Coastal Engineering 69 (2012) 42–66.

[28] P. L. Roe, Approximate riemann solvers, parameter vectors, and difference schemes, Journal of computational physics 43 (2) (1981) 357–372.

[29] R. J. LeVeque, et al., Finite volume methods for hyperbolic problems, Vol. 31, Cambridge university press, 2002.

[30] N. P. Waterson, H. Deconinck, Design principles for bounded higher-order convection schemes–a unified approach, Journal of Computational Physics 224 (1) (2007) 182–207.

[31] M. Kermani, A. Gerber, J. Stockie, Thermodynamically based moisture prediction using roe's scheme, 4th Conference of Iranian Aerospace Society, Amir Kabir University of Technology, Tehran, Iran 3 (2003) 1–10.

[32] A. G. Filippini, M. Kazolea, M. Ricchiuto, A flexible genuinely nonlinear approach for nonlinear wave propagation, breaking and run-up, Journal of Computational Physics 310 (2016) 381–417.

[33] G. Wei, J. T. Kirby, Time-dependent numerical code for extended boussinesq equations, Journal of waterway, port, coastal, and ocean engineering 121 (5) (1995) 251–261.

[34] M. Ricchiuto, A. G. Filippini, Upwind residual discretization of enhanced boussinesq equations for wave propagation over complex bathymetries, Journal of Computational Physics 271 (2014) 306–341.

[35] A. B. Kennedy, Q. Chen, J. T. Kirby, R. A. Dalrymple, Boussinesq modeling of wave transformation, breaking, and runup. i: 1d, Journal of waterway, port, coastal, and ocean engineering 126 (1) (2000) 39–47.

[36] C. Lacor, S. Smirnov, M. Baelmans, A finite volume formulation of compact central schemes on arbitrary structured grids, Journal of computational physics 198 (2) (2004) 535–566.

[37] M. Kazolea, M. Ricchiuto, On wave breaking for boussinesq-type models, Ocean Modelling 123 (2018) 16–39.

[38] S. Joshi, M. Kazolea, M. Ricchiuto, Parameter sensitivity for wave breaking closures in boussinesq-type models, Water WavesTo appear (2022).

[39] P. Lin, P. L.-F. Liu, A numerical study of breaking waves in the surf zone, Journal of fluid mechanics 359 (1998) 239–264.

[40] P. L.-F. Liu, J. Wen, Nonlinear diffusive surface waves in porous media, Journal of Fluid Mechanics 347 (1997) 119—139.